



HAL
open science

Influence of use conditions on heat transfer in an insulated box equipped with a phase change material

Tanathep Leungtongkum, Denis Flick, Nattawut Chaomuang, Alain Denis, Onrawee Laguerre

► **To cite this version:**

Tanathep Leungtongkum, Denis Flick, Nattawut Chaomuang, Alain Denis, Onrawee Laguerre. Influence of use conditions on heat transfer in an insulated box equipped with a phase change material. *Journal of Food Engineering*, 2023, 357, pp.111644. 10.1016/j.jfoodeng.2023.111644 . hal-04157392

HAL Id: hal-04157392

<https://hal.inrae.fr/hal-04157392v1>

Submitted on 10 Jul 2023

HAL is a multi-disciplinary open access archive for the deposit and dissemination of scientific research documents, whether they are published or not. The documents may come from teaching and research institutions in France or abroad, or from public or private research centers.

L'archive ouverte pluridisciplinaire **HAL**, est destinée au dépôt et à la diffusion de documents scientifiques de niveau recherche, publiés ou non, émanant des établissements d'enseignement et de recherche français ou étrangers, des laboratoires publics ou privés.

Copyright

Journal Pre-proof

Influence of use conditions on heat transfer in an insulated box equipped with a phase change material

Tanathep Leungtongkum, Denis Flick, Nattawut Chaomuang, Alain Denis, Onrawee Laguerre



PII: S0260-8774(23)00242-X

DOI: <https://doi.org/10.1016/j.jfoodeng.2023.111644>

Reference: JFOE 111644

To appear in: *Journal of Food Engineering*

Received Date: 26 April 2023

Revised Date: 18 June 2023

Accepted Date: 30 June 2023

Please cite this article as: Leungtongkum, T., Flick, D., Chaomuang, N., Denis, A., Laguerre, O., Influence of use conditions on heat transfer in an insulated box equipped with a phase change material, *Journal of Food Engineering* (2023), doi: <https://doi.org/10.1016/j.jfoodeng.2023.111644>.

This is a PDF file of an article that has undergone enhancements after acceptance, such as the addition of a cover page and metadata, and formatting for readability, but it is not yet the definitive version of record. This version will undergo additional copyediting, typesetting and review before it is published in its final form, but we are providing this version to give early visibility of the article. Please note that, during the production process, errors may be discovered which could affect the content, and all legal disclaimers that apply to the journal pertain.

© 2023 Published by Elsevier Ltd.

CRedit author statement

Tanathep Leungtongkum: Conceptualization, Methodology, Investigation, Validation, Formal analysis, Software, Writing - Original Draft Preparation and Visualization

Denis Flick: Methodology, Validation, Formal analysis, Writing - Review & Editing and Supervision.

Nattawut Chaomuang: Conceptualization, Methodology, Investigation, Validation, Formal analysis, Software, Writing - Original Draft Preparation, Visualization and Funding acquisition

Alain Denis: Investigation and Software

Onrawee Laguerre: Validation, Formal analysis, Writing - Review & Editing, Supervision, Project Administration, Funding acquisition

23 conditions. The maximum product temperature was lower for PCM at the top (6.6°C, AR ≈ 1)
 24 than for PCM on a sidewall (7.7°C, AR ≈ 1) and increased with AR (9.9°C, AR ≈ 1.7). A non-
 25 linear relation between ambient temperature and product temperature was observed with the
 26 maximum product temperature from 5.2°C (10°C ambient) to 9.1°C (30°C ambient). The
 27 influence of spacing beneath the product was negligible despite different airflow patterns.
 28 Simple equations were proposed to predict the maximum storage time and mean temperature
 29 in the box enabling us to study the influence of PCM and product mass, melting point, box
 30 insulation and ambient temperature.

31 **Keywords:** Insulated box, Phase Change Material, Airflow, Heat Transfer, Food Cold Chain

32 Nomenclature

33	A	Exchange area [m ²]
34	AR	Aspect ratio of box = height/width [-]
35	C_p	Specific heat [J·kg ⁻¹ ·K ⁻¹]
36	e	Wall thickness [m]
37	h	Convective heat transfer coefficient [W·m ⁻² ·K ⁻¹]
38	L	Characteristic length [m]
39	L_f	Latent heat of fusion of PCM [J·kg ⁻¹]
40	\dot{m}	Mass flow rate of air [kg·s ⁻¹]
41	m	Mass [kg]
42	t	Time [s]
43	t_{max}	Maximum storage time [s]
44	T	Temperature [°C]
45	T_m	Melting temperature of PCM (~ 0°C)
46	T_{amb}	Ambient temperature [°C]

- 47 T^* Dimensionless temperature = $\frac{T - T_m}{T_{amb} - T_m}$ [-]
- 48 ΔT Largest temperature difference [°C]
- 49 U Overall heat transfer coefficient between ambient and product surface through
50 box insulation [$\text{W}\cdot\text{m}^{-2}\cdot\text{K}^{-1}$]
- 51 x, y, z Coordinate [m]

52 Greek letters

- 53 α_c Dimensionless heat transfer coefficient at cold wall = $\exp\left(-\frac{A_c h_c}{\dot{m} C_{p,air}}\right)$ [-]
- 54 α_w Dimensionless heat transfer coefficient at warm walls = $\exp\left(-\frac{A_w U}{\dot{m} C_{p,air}}\right)$ [-]
- 55 β Ratio of thermal resistance at cold and at warm walls = $\frac{A_w U}{A_c h_c}$ [-]
- 56 ρ Density [$\text{kg}\cdot\text{m}^{-3}$]
- 57 τ Thermal time constant [s]
- 58 λ Thermal conductivity [$\text{W}\cdot\text{m}^{-1}\cdot\text{K}^{-1}$]

59 Subscript

- 60 *air* Air
- 61 *ave* Average value
- 62 *c* Cold surface/walls
- 63 *ini* Initial value
- 64 *max* Maximum value
- 65 *min* Minimum value
- 66 *p* Product
- 67 *pcm* Phase change material
- 68 *w* Warm surface/walls

69 **1. Introduction**

70 Insulated boxes equipped with a Phase Change Material (PCM) are attracting particularly for
71 the last mile delivery of small quantities of temperature-sensitive food and pharmaceutical
72 products. This is due to the simple implementation, low cost and flexibility related to several
73 box designs with different volumes ranging from 5 L to more than 300 L. Several parameters
74 have an influence on the internal temperature profiles such as box characteristics (dimensions,
75 aspect ratio, insulation), PCM (melting point, mass, position), product (thermal properties,
76 mass, compactness) and operating condition (ambient temperature, transport duration).
77 Because of the complex interactions between these parameters, they need to be considered
78 together to avoid temperature abuse during delivery.

79 The temperature evolution inside an insulated box equipped with PCM loaded by real
80 food/food model was investigated experimentally and numerically by several authors and
81 summarized in Leungtongkum et al. (2022). In general, the product located at the corners of
82 the box has the highest temperature (Laguerre et al., 2018; Margeirsson et al., 2012). Du et al.
83 (2020) have compared the effect of PCM at the top, bottom, and all sidewalls on internal
84 temperature evolution. The authors found that placing PCM at the bottom generated the highest
85 internal temperature and the highest temperature difference between the min and max values.
86 For high-value products like vaccines, five or six PCM plates are placed on the box walls to
87 directly compensate the heat losses through the walls by PCM melting. This allows assuring
88 the preservation of the recommended temperature (Kacimi & Labranque, 2019) but the useful
89 volume for the product is significantly reduced, thus, this practice may not be suitable for low
90 cost product like food.

91 For simplification purposes, several studies assumed conduction only in the air, the product
92 and the wall (Du et al., 2020; Paquette et al., 2017; Xiaofeng & Xuelai, 2021). To represent the
93 real phenomena, Rincón-Casado et al. (2017) developed a numerical model considering

94 conduction and natural convection to predict the temperature profile and airflow pattern in an
95 empty cavity while Leporini et al. (2018) also took radiation into account. Recently, some
96 numerical studies considered natural convection of internal air and of melted PCM (Burgess et
97 al., 2022; Calati et al., 2022; Rahimi-Khoigani et al., 2023).

98 Various phenomena are involved simultaneously in an insulated box equipped with PCM:
99 conduction inside the product, the PCM and the walls of the box, convection between air and
100 product/PCM, and between the external air and the box, radiation between walls, phase change
101 during PCM melting and food quality evolution. Under natural convection as that in an
102 insulated box, these three heat transfer modes (conduction, convection and radiation) are of the
103 same order of magnitude in terms of heat flux (Laguerre & Flick, 2004). However, only a few
104 studies considered all of them according to the difficulty in measuring low air velocities
105 (Miroshnichenko & Sheremet, 2018). In fundamental studies of natural convection in a closed
106 cavity, two walls are generally at imposed temperatures (cold and warm) while the other walls
107 are adiabatic, and most of them investigated empty cavities (Leporini et al., 2018; Zhang et al.,
108 2015). PCM was used as a thermal energy storage in an empty cavity (Labihi et al., 2017;
109 Moreno et al., 2020). Choi et al. (2015) and Lee et al. (2016) conducted numerical studies of a
110 rectangular cavity filled with a circular cylinder (cylinder diameter /cavity size = 0.125). Some
111 studies have investigated cavities filled with a porous medium (particle diameter/box width <
112 0.01), e.g., Ataei-Dadavi et al. (2019). The results of these studies cannot be applied to our case
113 where only one wall (PCM container) is at almost constant temperature and all the other walls
114 of the box are non-adiabatic. Moreover, a porous medium approach is not appropriate to our
115 study, since the ratio between product diameter and box width is ≥ 0.1 , thus, different airflow
116 pattern.

117 The strength of our work is that it is the first experimental study concerning the measurement
118 of airflow patterns and air velocity in an insulated box with PCM at different locations by using

119 an optical technique (PIV). Some results were already presented in a previous article
120 (Leungtongkum et al., 2023a) for a limited number of configurations. The present article
121 investigates many more parameters: aspect ratio, ambient temperature, initial product
122 temperature and air gap underneath the product. From a practical point of view, this article also
123 proposes simple equations to predict the maximum storage time, the equilibrium temperature
124 and temperature heterogeneity at thermal stable condition enabling to study the influence of
125 PCM mass, melting point, box insulation and ambient temperature. These equations are easy to
126 use and they would be useful for stakeholders, for example, to choose the box insulation and
127 the PCM mass according to the product to transport, duration and ambient temperature during
128 the supply chain.

129 It is to be emphasized that certain experimental data presented in this article were used for a
130 thermal model development based on the zonal approach. This model takes into account
131 conduction, convection and radiation inside an insulated box (Leungtongkum et al., 2023b).

132 **2. Material and methods**

133 The material and methods described in detail in Leungtongkum et al. (2023a) are presented
134 succinctly below.

135 **2.1 Experimental setup**

136 For thermal study, the box is a 45-L commercialized multilayer insulated box (Manutan SA,
137 Gonesse, France). In fact, commercialized boxes are available in various sizes (from less than
138 5 L to more than 300 L). For meat, a highly perishable food, the boxes generally do not exceed
139 50 L. To be close to real situations, we chose a 45-L box in our study. For airflow study, the
140 box has the same dimensions and wall structure as the one for thermal study, but two side walls
141 are replaced by triple-glazed windows (3 glass panes each with a thickness of 4 mm, 2 argon-
142 filled 10-mm gaps) to allow the entrance of laser sheet and the image capture by a camera. The

143 overall heat transfer coefficient of the walls of these two boxes is almost the same ($0.89 \text{ W}\cdot\text{m}^{-2}\cdot\text{K}^{-1}$).
144

145 The PCM container, made of polypropylene (3.5-mm thickness), had external dimensions 460
146 mm x 280 mm x 50 mm and was filled with 3.5 kg of tap water (melting point $\sim 0^\circ\text{C}$). The
147 thermophysical properties of PCM (water in this study), in both liquid and solid state along
148 with its enthalpy of melting is shown in Table 1. Since the form of food is diverse, Tylose
149 packs are used as test product (dimensions of a pack 200 mm x 100 mm x 50 mm) as that used
150 in standard tests for thermal performance of cold equipment. The physical properties of this
151 test product are close to the ones of meat (Table 1). This configuration (compact load with air
152 gaps between load and box walls) was studied by several authors (Ohkawara et al., 2012; Zhao
153 et al., 2019).

154 The box can be placed horizontally (AR , height/width ≈ 1) or vertically ($AR \approx 1.7$), making it
155 possible to study the effect of the aspect ratio on heat transfer and the airflow pattern. The
156 effect of the air space underneath the product was studied by placing the test product on a
157 perforated support made of galvanized steel (length x width x height = 350 x 150 x 20 mm and
158 150 x 150 x 20 mm for a horizontal and a vertical box, respectively). An example of
159 experimental setup for a horizontal box with PCM on a side wall is shown in Figure 1.

160 **2.2 Thermal study**

161 To assure the homogeneous initial PCM temperature, a PCM slab was placed horizontally in a
162 freezer set at a temperature of -2°C for at least 48 h before each experiment. To assure the
163 homogeneous initial product temperature, sixteen packs of test product were placed in a
164 polystyrene box and stored in a domestic refrigerator set at a temperature of 4°C or 10°C for
165 at least 24 h before each experiment. In this manner, the product temperature is not influenced
166 by the air temperature fluctuation due to “on” and “off” compressor working cycles.

167 Temperatures of PCM, air, and test product in the loaded box (Figure 1) were measured at 35
168 positions located in the middle plane ($x = 250$ mm) every 30 s from 400 min. to 600 min. after
169 closing the box to assure the stabilization of temperature during the measurement. The
170 temperature contour map was drawn by MATLAB by interpolation from 30 measured points.
171 More detail on temperature measurements can be found in Leungtongkum et al. (2023a).

172 It is to be emphasized that the T-type thermocouples were previously calibrated at -10°C , 0°C ,
173 10°C , 20°C and 30°C and allowed the measurement precision of $\pm 0.2^{\circ}\text{C}$.

174 Table 2 describes the experimental conditions (cf. the detailed description in Section 2.4).
175 Conditions 1, 2, 9 and 10 were done twice to verify the repeatability of the results. These
176 conditions are notified by “*” in Table 2. Since the result repeatability was observed in these
177 conditions (standard deviation $\sim 0.2^{\circ}\text{C}$), the other ones reported in this Table were done only
178 once allowing a large number of experimental conditions to be fulfilled.

179 **2.3. Airflow study**

180 Non-intrusive air velocity measurements were achieved by PIV (Particle Image Velocimetry).
181 The PIV device is constituted of three components: a double-pulsed Nd:YLF laser (527 nm
182 wavelength, 10 mJ pulse energy), a high-speed 12-bit CMOS video camera (Photron,
183 FASTCAM SA3; 1024×1024 pixels in resolution) fitted with a lens (Sigma; 105 mm, $f/1:2.8$)
184 and a programmable timing unit (PTU-X) to ensure synchronization of the laser and the
185 camera. Visualization of the airflow pattern is possible by the scattering of smoke particles
186 during laser pulses. Oil-based particles (mean diameter $0.3 \mu\text{m}$) were generated using a smoke
187 machine (Antari, F-80Z). Based on our calibration, the image size was $115.5 \text{ mm} \times 115.5 \text{ mm}$.
188 The positions of the measured windows partially overlapped with the neighboring one using
189 the displacement system. Finally, the air velocity field over the whole area of the plane could
190 be developed.

191 For each measured window, 500 pairs of images were recorded every 20 ms with a time interval
192 of 900 μ s between two images of the same pair (between two laser pulses) with the total
193 measurement duration of 10 s. After capturing all the images, instantaneous airflow vectors
194 were calculated using a cross-correlation method with a multi-pass correlation algorithm
195 (Raffel et al., 2007). The distance between two vectors was around 0.9 mm in both horizontal
196 and vertical directions. After 500 instantaneous vector fields had been attained, the mean
197 velocity field of each measured window was calculated. More detail on PIV system, image
198 acquisition, image post-processing and experimental protocol can be found in Leungtongkum
199 et al. (2023a).

200 **2.4 Experimental conditions**

201 Table 2 summarizes the investigated experimental conditions: position of PCM, aspect ratio of
202 the box, ambient temperature, initial test product temperatures and its position. The pictograms
203 were introduced for further reference. The studied conditions (except PCM position) are new
204 in comparison to the ones presented in Leungtongkum et al. (2023a).

205 **3. Results and discussions**

206 In addition to the results presented in our previous work (Leungtongkum et al., 2023a), this
207 article focuses on the influence of box designing and operating parameters on temperature and
208 air velocity fields: box aspect ratio and PCM position (Figure 2), external and initial product
209 temperatures (Figure 3), space beneath the test product (Figure 4). These influences on the
210 average, min and max temperatures of product core/surface and air at stable condition are
211 summarized in Table 3. To complete the data at stable condition, the time-temperature
212 evolutions at different positions are presented in Figure 5, the analysis of the time to reach
213 stable condition (thermal time constant) quantitatively shows the importance of heat fluxes by
214 conduction and convection. The experimental results shown in Figure 6 show the effect of the

215 amount of PCM on product temperature. Finally, simple equations are proposed to predict the
216 maximum storage time in function of box insulation, PCM mass, melting point, product mass,
217 ambient temperature.

218 **3.1 Effect of the aspect ratio**

219 Figure 2 shows the airflow pattern and the temperature field on the middle plane of horizontal
220 and vertical loaded boxes with PCM on the right side. The absence of air velocity in the gap
221 between the test product and PCM of the horizontal box can be explained by the impossibility
222 of laser sheet projection in this zone, thus, no PIV measurement. The same reason explains the
223 absence of air velocity in the gap below the test product of the vertical box.

224 When PCM was on the side (Figures 2a and 2c), air flows downwards close to PCM and flows
225 upwards close to the opposite vertical wall. In the gap between the test product and the box
226 wall (left side), the upward maximal velocity was similar in both cases ($\sim 0.11 \text{ m}\cdot\text{s}^{-1}$, with an
227 uncertainty of $3 \times 10^{-3} \text{ m}\cdot\text{s}^{-1}$). Comparison is not possible in the gap between the PCM and the
228 test product. However, in the vertical box, the maximal downward velocity ($0.13 \text{ m}\cdot\text{s}^{-1}$, with
229 an uncertainty of $3 \times 10^{-3} \text{ m}\cdot\text{s}^{-1}$) was higher than the maximal upward velocity ($0.11 \text{ m}\cdot\text{s}^{-1}$, with
230 an uncertainty of $3 \times 10^{-3} \text{ m}\cdot\text{s}^{-1}$). This is because downward flow occurs only along the PCM,
231 whereas upward flow occurs not only along the opposite wall but also along the two other
232 vertical box walls (results not shown).

233 Regarding the temperature field (Figures 2a' and 2c'), increasing the height of the box did not
234 change the coldest and warmest positions. The coldest spot was located at the bottom close to
235 the PCM surface and the warmest spot was at the top close to the opposite side wall.

236 Table 3 summarizes the average temperatures observed between 400 and 600 min. considered
237 as a stable period. In the pictograms, the cold/warm spot locations for air and the product are
238 shown. This table distinguishes the temperature of air, of the product surface and of the product

239 core in terms of average, maximum and minimum values. In the following section, we will
240 focus on the average product core value, $T_{pc, ave}$ and the maximum product temperature (core
241 or surface), $T_{p, max}$, because of the importance for product quality and the sanitary risk (on the
242 average and for the highest temperature location). Indeed, the minimum product temperature
243 was always positive (no freezing risk) since PCM was initially at a temperature of -2°C and
244 melted near 0°C . To complement these findings, we will also consider the air temperature
245 heterogeneity: $\Delta T_{air} = T_{air, max} - T_{air, min}$. Since the standard deviation (SD) between replicates
246 for average product (core or surface, 4 positions each) temperatures is around 0.2°C (see Table
247 3), we should consider that a difference of less than about 0.5°C does not exert a significant
248 impact on product quality evolution.

249 Increasing the height of the box significantly led to higher product temperatures and greater air
250 temperature heterogeneity:

251 Horizontal box: $T_{pc, ave} = 5.8^{\circ}\text{C}$, $T_{p, max} = 7.7^{\circ}\text{C}$, $\Delta T_{air} = 6.0^{\circ}\text{C}$, SD of $T_{air} = 2.2^{\circ}\text{C}$

252 Vertical box: $T_{pc, ave} = 7.8^{\circ}\text{C}$, $T_{p, max} = 9.9^{\circ}\text{C}$, $\Delta T_{air} = 7.5^{\circ}\text{C}$, SD of $T_{air} = 3.0^{\circ}\text{C}$

253 A higher aspect ratio (height/width) leads to larger temperature differences between the top
254 and the bottom. Thus, it is recommended to limit the height of insulated boxes. In fact,
255 increasing the height should increase convective heat transfer between PCM and air (according
256 to Nu-Ra correlations) but the air pathway along the box walls is longer and thermal
257 stratification is stronger. Finally, under conditions close to ours, these different phenomena
258 lead to higher average temperature and temperature heterogeneity for higher aspect ratio.

259 **3.2 Effect of the PCM position**

260 The effect of PCM position on temperature and air velocity fields of a horizontal box are shown
261 in Figure 2. For PCM at top, upward flow was observed near the left box wall and also near
262 the top of test product but only a very weak downward flow (dashed arrow A in Figure 2b) was

263 noticed in the left gap. In fact, flow was asymmetric: under the PCM, cold air flows
 264 preferentially towards the right gap where downward flow certainly dominates, whereas
 265 upward flow dominates in the left gap.

266 The temperature distribution on the middle plane (Figure 2b') also shows a dissymmetry of air
 267 and product temperatures. Air was at a temperature of around 5.2°C in the right gap and around
 268 6.6°C in the left gap. This confirms the hypothesis of asymmetric airflow.

269 Placing PCM at the top allowed lower average temperature and lower air temperature
 270 heterogeneity:

271 PCM on the side: $T_{pc, ave} = 5.8^{\circ}\text{C}$, $T_{p, max} = 7.7^{\circ}\text{C}$, $\Delta T_{air} = 6.0^{\circ}\text{C}$, SD of $T_{air} = 2.2^{\circ}\text{C}$

272 PCM at the top: $T_{pc, ave} = 5.4^{\circ}\text{C}$, $T_{p, max} = 6.6^{\circ}\text{C}$, $\Delta T_{air} = 2.5^{\circ}\text{C}$, SD of $T_{air} = 1.1^{\circ}\text{C}$

273 Hence, placing PCM at the top is more appropriate for food transport and this configuration
 274 was used for further study of the influence of ambient and initial test product temperatures.

275 3.3 Effect of ambient temperature

276 Figure 3 presents the temperature field of the loaded box with a 20-mm air gap underneath and
 277 PCM at the top under ambient temperatures of 10°C (Figure 3a), 20°C (Figure 3b) and 30°C
 278 (Figure 3c). To compare the effect of different ambient temperatures on measured
 279 temperatures, the dimensionless temperature T^* was defined (Equation 1).

$$280 \quad T^* = \frac{T - T_m}{T_{amb} - T_m} \quad (1)$$

281 where T is the average value of the temperatures measured between 400 min. and 600 min.

282 Logically, increasing ambient temperature led to a higher product temperature and greater air
 283 temperature heterogeneity:

284 $T_{amb} = 10^{\circ}\text{C}$: $T_{pc, ave} = 4.3^{\circ}\text{C}$ ($T^*_{pc, ave} = 0.43$), $T_{p, max} = 5.2^{\circ}\text{C}$, $\Delta T_{air} = 1.7^{\circ}\text{C}$, SD of $T_{air} = 0.5^{\circ}\text{C}$

285 $T_{amb} = 20^{\circ}\text{C}$: $T_{pc, ave} = 5.4^{\circ}\text{C}$ ($T^*_{pc, ave} = 0.27$), $T_{p, max} = 6.6^{\circ}\text{C}$, $\Delta T_{air} = 2.5^{\circ}\text{C}$, SD of $T_{air} = 1.1^{\circ}\text{C}$

286 $T_{amb} = 30^{\circ}\text{C}$: $T_{pc, ave} = 7.2^{\circ}\text{C}$ ($T_{pc, ave}^* = 0.24$), $T_{p, max} = 9.1^{\circ}\text{C}$, $\Delta T_{air} = 4.8^{\circ}\text{C}$, SD of $T_{air} = 1.6^{\circ}\text{C}$

287 The positions of the coldest and warmest spots were the same for all ambient temperatures.

288 One could expect that in terms of dimensionless temperature, the results would be the same,

289 but this is not the case when applied to the average core temperature (T^* varying between 0.43

290 and 0.24). This can be due to the non-linearity of heat fluxes versus temperature difference in

291 free convection: fluid flow and consequently the convective heat transfer coefficient which

292 depends on the temperature difference. This was effectively observed with more noticeable

293 downward airflow at an ambient temperature of 30°C (result not shown). This can also be due

294 to the influence of the initial product temperature which is different in dimensionless terms for

295 the three ambient temperatures (thermal inertia effect). Thus, a simple linear extrapolation

296 cannot be applied for different ambient temperatures. For example, a 50% increase in the

297 difference between the ambient temperature and the PCM melting temperature does not

298 necessarily lead to a 50% higher product temperature. Similar results were obtained for PCM

299 on the side (see Table 3, conditions 1 and 4). Physical-based models, e.g. zonal model or CFD,

300 could be used to analyze the effect of ambient temperature on temperature heterogeneity and

301 temperature evolution.

302 **3.4 Effect of the initial test product temperature**

303 Figure 3d presents the temperature field for an initial test product temperature of 10°C and

304 PCM at the top under ambient conditions of 20°C . By comparing Figures 3b and 3d, it was

305 observed that a higher initial test product temperature led to a higher product temperature:

306 $T_{pc, ini} = 4^{\circ}\text{C}$: $T_{pc, ave} = 5.4^{\circ}\text{C}$ ($T_{pc, ave}^* = 0.27$), $T_{p, max} = 6.6^{\circ}\text{C}$, $\Delta T_{air} = 2.5^{\circ}\text{C}$, SD of $T_{air} = 1.1^{\circ}\text{C}$

307 $T_{pc, ini} = 10^{\circ}\text{C}$: $T_{pc, ave} = 8.0^{\circ}\text{C}$ ($T_{pc, ave}^* = 0.40$), $T_{p, max} = 9.2^{\circ}\text{C}$, $\Delta T_{air} = 2.8^{\circ}\text{C}$, SD of $T_{air} = 0.9^{\circ}\text{C}$

308 Theoretically, the same results would be expected under steady state conditions, whatever the

309 initial test product temperature if the same ambient temperature and PCM melting point are

310 applied. This means that even after 8 h (on an averaged basis between 400 and 600 min.),
311 steady state was not reached. This is highlighted in Section 3.6.

312 Similar results were obtained for PCM on the side (see Table 3, conditions 1 and 7). Concerning
313 application aspects, placing a load with a high initial temperature in packaging is not
314 recommended for food transport because PCM should only serve to maintain the product
315 temperature, not to cool it.

316 **3.5 Effect of a space beneath the test product**

317 Figure 4 illustrates the air velocity field for the box with PCM at the top and on the side with
318 a 20-mm gap underneath the test product (Figure 4a and Figure 4c) and without a gap (Figure
319 4b and Figure 4d). This gap is expected to ensure better air circulation and avoid direct heat
320 conduction from the bottom wall to the product.

321 When PCM was at the top (Figures 4a and 4b), the airflow pattern was quite similar with and
322 without gap. From Table 3, for PCM at the top, it appears that the influence of gap beneath the
323 test product on the product temperature is not significant.

324 With a 20-mm gap: $T_{pc, ave} = 5.4^{\circ}\text{C}$, $T_{p, max} = 6.6^{\circ}\text{C}$, $\Delta T_{air} = 2.5^{\circ}\text{C}$, SD of $T_{air} = 1.1^{\circ}\text{C}$

325 Without gap: $T_{pc, ave} = 5.6^{\circ}\text{C}$, $T_{p, max} = 7.2^{\circ}\text{C}$, $\Delta T_{air} = 2.6^{\circ}\text{C}$, SD of $T_{air} = 1.0^{\circ}\text{C}$

326 When PCM was on the side (Figure 4c and 4d), the maximum air velocity was slightly higher
327 with the gap ($0.13 \text{ m}\cdot\text{s}^{-1}$, with an uncertainty of $3 \times 10^{-3} \text{ m}\cdot\text{s}^{-1}$ and $0.10 \text{ m}\cdot\text{s}^{-1}$, with an uncertainty
328 of $9 \times 10^{-3} \text{ m}\cdot\text{s}^{-1}$ in the box with 20-mm gap underneath and without a gap, respectively). In
329 spite that the presence of gap led to better air circulation, the influence on product temperature
330 was not obvious. From Table 3, for PCM on the side:

331 With a 20-mm gap: $T_{pc, ave} = 5.8^{\circ}\text{C}$, $T_{p, max} = 7.7^{\circ}\text{C}$, $\Delta T_{air} = 6.0^{\circ}\text{C}$, SD of $T_{air} = 2.2^{\circ}\text{C}$

332 Without gap: $T_{pc, ave} = 5.8^{\circ}\text{C}$, $T_{p, max} = 7.5^{\circ}\text{C}$, $\Delta T_{air} = 7.3^{\circ}\text{C}$, SD of $T_{air} = 2.5^{\circ}\text{C}$

333 Since the presence of gap has insignificant influence on product temperature, it is more
334 practical to load the product directly onto the bottom of the box without providing a gap.

335 **3.6 Temperature evolution**

336 Figure 5 presents the temperature evolution at several positions in a loaded horizontal box with
337 PCM on the side after the lid was closed. The internal wall (TC1), internal air (TC2, TC5 and
338 TC8) and PCM surface temperatures (TC9) decreased rapidly over a period of around 60 min.
339 before gradually increasing, while the surface and core temperatures of the test product (TC3,
340 TC4, TC6 and TC7) increased slowly over a period of 1100 min. (18 h).

341 The difference in temperature evolution of the walls of the box and the test product can be
342 explained by their thermal inertia, diffusivity and convective heat exchange with air. The Biot
343 number (Bi) was used to compare the effect of the internal and external thermal resistance of
344 these materials, as defined in Equation. 2:

$$345 \quad Bi = \frac{hL}{\lambda} \quad (2)$$

346 where L is the characteristic length represented by the thickness of the inner polypropylene
347 layer (3.5 mm) for a wall of the box (considering that heat exchanged only with one side) and
348 by the half thickness of the test product (100 mm). Due to natural convection inside the box,
349 the order of magnitude of the heat transfer coefficient is approximately $5 \text{ W}\cdot\text{m}^{-2}\cdot\text{K}^{-1}$.

350 Consequently, the Biot number is 0.146 for polypropylene and 0.98 for the test product. Hence,
351 the thermal resistance of the internal wall could be neglected, while that of the test product is
352 of the same order of magnitude as the external thermal resistance.

353 The thermal time constant related to conduction can be estimated by Equation. 3 (Bergman et
354 al., 2011).

355
$$\tau_{conduction} = \frac{\rho C_p L^2}{\lambda} \quad (3)$$

356 Similarly, the thermal time constant related to convection can be estimated by Equation. 4
357 (Bergman et al., 2011).

358
$$\tau_{convection} = \frac{\rho C_p L}{h} \quad (4)$$

359 For the internal wall, the thermal time constants for conduction and convection are 179 s (3
360 min.) and 1230 s (20 min.), respectively. It can be concluded that the delay in temperature
361 evolution of the internal walls was mainly caused by convection between adjacent air and the
362 walls.

363 For the test product, the thermal time constants of conduction and convection are 70800 s (>
364 19 h) and 72200 s (> 20 h), respectively. Thus, both heat conduction and convection play an
365 important role in the temperature evolution, and this explains the temperature difference
366 between the core, the surface of test product and the adjacent air.

367 The thermal time constants of the test product are much longer than those of the internal wall
368 and this results in a different rate of temperature evolution.

369 According to Figure 5, the internal temperature of PCM (TC10) increased after 800 min. (~13
370 h) indicating that PCM was melted. The temperature of the other components thus increased.

371 In view of the thermal time constant for the product, PCM is melted before the product reaches
372 thermal equilibrium, so there was no steady state in this condition. One could consider a
373 hypothetical equilibrium temperature which would be reached after a long period by assuming
374 that PCM is still at the melting temperature everywhere. Roughly, for horizontal boxes, for
375 PCM either at the top or on the side:

376 $T_{pc, ini} = 4^{\circ}\text{C}$: after 8 h, $T_{pc, ave}$ is at around 5.5°C and the temperature is still rising

377 $T_{pc, ini} = 10^{\circ}\text{C}$: after 8 h, $T_{pc, ave}$ is at around 8.5°C and it is still decreasing

378 Therefore, the equilibrium temperature should be around 7°C.

379 In practice, to be able to compare the performances of insulated boxes equipped with PCM, the
380 experiments should be carried out under the same loading conditions (mass and initial
381 temperature), ambient temperature and duration of temperature measurement.

382 **3.7 Effect of the amount of PCM on the test product temperature evolution and maximum** 383 **storage time**

384 This section describes a comparison of the experimental test product core temperature evolution
385 (average of four measurements at different locations) for 3 amounts of PCM: 0 kg, 1.7 kg (about
386 10% of the product mass), and 3.5 kg (about 20% of the product mass) (Figure 6a). This
387 experiment was undertaken for PCM located on a sidewall of a horizontal box loaded with the
388 test product at an initial temperature of 4°C and 20°C ambient temperature. The higher amount
389 of PCM lowered the rate of temperature increase. For example, during the first 2 h, this rate
390 was 1.13°C·h⁻¹, 0.58°C·h⁻¹ and 0.34°C·h⁻¹, for 0 kg, 1.7 kg and 3.5 kg of PCM, respectively.

391 Figure 6b presents the relationship between the maximum product storage time (t_{max}) and the
392 amount of PCM. This maximum storage time is defined as the duration during which the
393 product remains below $T_{p,max} = 8^{\circ}\text{C}$, which is the maximum temperature value for the storage
394 of certain chilled foods. The higher the amount of PCM, the higher the maximum storage time:
395 370 min. (for 0 kg), 944 min. (for 1.7 kg) and 1373 min. (for 3.5 kg). The results obtained in
396 terms of product temperature evolution and maximum storage time confirm the benefit of PCM
397 for food preservation as reported by Zhao et al. (2019) for strawberries. These authors showed
398 that the use of PCM allowed less weight loss and greater product firmness in comparison with
399 the case where PCM was not used.

400 To determine approximately the maximum storage time as a function of the amount of PCM,
 401 the following heat balance equation can be used:

$$402 \quad m_p C_{p,p}(T_{p,max} - T_{p,ini}) + m_{pcm} L_f = UA \left(T_{amb} - \frac{T_{p,ini} + T_{p,max}}{2} \right) t_{max} \quad (5)$$

403 where U is the overall heat transfer coefficient of the box [$W \cdot m^{-2} \cdot K^{-1}$]
 404 and A is the exchange area [m^2]

405 The overall heat transfer coefficient of the box can be related to the thicknesses (e_k) and
 406 conductivities (λ_k) of the box wall materials (of index k) as shown in Equation 6 (assuming
 407 negligible convective heat transfer resistances).

$$408 \quad \text{Thus, } U = \frac{1}{\sum_k \frac{e_k}{\lambda_k}} \quad (6)$$

409 Equation 5 assumes that PCM is completely melted when $T_{p,max}$ is reached and that the internal
 410 temperature is close to the average test product temperature.

411 Based on these assumptions, Equation 5 becomes:

$$412 \quad t_{max} = t_{max,0} \left(1 + \alpha \frac{m_{pcm}}{m_p} \right) \quad (7)$$

413 where $t_{max,0}$ is the maximum storage time of the box without PCM defined as

$$414 \quad t_{max,0} = \frac{m_p C_{p,p}(T_{p,max} - T_{p,ini})}{UA \left(T_{amb} - \frac{T_{p,ini} + T_{p,max}}{2} \right)} \quad [s]$$

$$415 \quad \text{and } \alpha = \frac{L_f}{C_{p,p}(T_{p,max} - T_{p,ini})} \quad [-]$$

416 This indicates a linear relationship between the maximum storage time and the amount of PCM
 417 as shown in Figure 6b.

418 In practice, for all types of boxes, it is suggested that this type of experiment should be
 419 conducted, at a fixed ambient temperature, without and with a given amount of PCM to
 420 determine $t_{max,0}$ and α . The influence of other parameters could be approximated according to

421 Equations 5 and 7. For example, it is expected that the maximum storage time is inversely
 422 proportional to the difference between the ambient temperature (T_{amb}) and the internal
 423 temperature considered as the average test product temperature ($\frac{T_{p,ini} + T_{p,max}}{2}$).

424 3.8 Expected influence of insulation on temperature level and heterogeneity

425 The present study considered only one insulation configuration. This section aims to predict the
 426 effect of changing the insulation by using a basic approach. This effect is the determining factor
 427 for the temperature distribution in insulated boxes equipped with PCM (Paquette et al., 2017).
 428 To illustrate the influence of the box insulation, the analysis presented below concerns the box
 429 with PCM on the side where a higher temperature level and greater heterogeneity were
 430 observed.

431 As a first approach, the steady state mean temperature in the box (T_{mean}) could be obtained from
 432 the following energy balance (Equation 8):

$$433 \quad A_c h_c (T_{mean} - T_m) = A_w U (T_{amb} - T_{mean}) \quad (8)$$

434 where A_c and A_w are the surface area of warm (insulated) and cold (PCM) walls [m^2],

435 h_c is the heat transfer coefficients between product and PCM surface [$W \cdot m^{-2} \cdot K^{-1}$],

436 U is the overall heat transfer coefficient between ambient and product surface
 437 through box insulation [$W \cdot m^{-2} \cdot K^{-1}$] and

438 T_m and T_{amb} are the melting temperature of the PCM and the external temperature,

439 respectively [$^{\circ}C$].

440 When the box is horizontal, in our case $\beta = (A_w U) / (A_c h_c) \approx 0.54$ with $T_m = 0^{\circ}C$, $T_{amb} = 20^{\circ}C$ and
 441 $T_{mean} \approx 7^{\circ}C$. Since $A_w / A_c = 4.3$ and $h_c / U \approx 8$; therefore, if insulation is improved by 30%, (i.e.,
 442 U divided by 1.3), the mean temperature should decrease from $7^{\circ}C$ to $5.9^{\circ}C$.

443 To obtain an estimation of temperature heterogeneity, it can be assumed that air flows, with a
 444 mass flowrate \dot{m} , first along the PCM, where its temperature decreases to T_{min} , then along the
 445 warm walls, where the temperature rises to T_{max} . The following equations characterize these
 446 heat exchange phenomena (Equations 9 and 10):

$$447 \quad T_{air,min} - T_m = \alpha_c (T_{air,max} - T_m) \quad (9)$$

$$448 \quad \text{where} \quad \alpha_c = \exp\left(-\frac{A_c h_c}{\dot{m} C_{p,air}}\right)$$

$$449 \quad T_{amb} - T_{air,max} = \alpha_w (T_{amb} - T_{air,min}) \quad (10)$$

$$450 \quad \text{where} \quad \alpha_w = \exp\left(-\frac{A_w U}{\dot{m} C_{p,air}}\right) = \alpha_c^\beta$$

$$451 \quad \text{Therefore;} \quad T_{air,max} - T_{air,min} = \frac{(1-\alpha_c)(1-\alpha_w)(T_{amb}-T_m)}{(1-\alpha_c\alpha_w)} \quad (11)$$

452 For the academic case of a square cavity with one vertical cold wall (T_c), one vertical warm
 453 wall (T_w) and adiabatic horizontal walls, Raithby & Hollands (1998) found that $T_{air,max} -$
 454 $T_{air,min} \approx 0.5(T_w - T_c)$ for the cavity with a low aspect ratio ($AR < 40$) which is often the
 455 case of insulated boxes (T_w and T_c are the temperature of warm wall and cold wall, respectively).
 456 If our basic approach is applied to this case, it can be estimated that $\alpha_c \approx 1/3$.

457 In our case ($\beta \approx 0.54$), it was calculated that $T_{air,max} - T_{air,min} \approx 7.4^\circ\text{C}$ which is comparable
 458 to the observed values. If insulation is improved by 30% for example (β divided by 1.3), the
 459 temperature heterogeneity should decrease from 7.4°C to 6.1°C .

460 This basic approach does not take into account the interaction with the test product especially
 461 during the unsteady period, radiation, complex flow etc., but it allows a rough estimation of the
 462 influence of insulation. It also highlights the influence of the air mass flowrate (\dot{m}) and the heat
 463 transfer (h_c) along the PCM on the temperature level and heterogeneity.

464 **4. Conclusion and perspectives**

465 This study investigated airflow and temperature fields inside an insulated box equipped with
466 PCM loaded with test product (Tylose slabs). PCM position significantly affected airflow
467 patterns, air temperature profile, product temperature homogeneity, and average product
468 temperature. When PCM was on a sidewall, the coldest position was at the bottom, close to the
469 PCM surface, and the warmest one was at the top close to the opposite vertical wall. When
470 PCM was at the top, the lowest product temperature was located at the top, while the highest
471 one was at the bottom, and slightly lower air and product temperatures were observed.
472 Increasing the box aspect ratio (higher box) led to a higher product temperature and greater
473 temperature heterogeneity (at least for PCM on the side). The non-linear correlation between
474 ambient temperature and product temperature can be explained by the non-linearity of free
475 convection and the product thermal inertia. An insignificant influence of the initial product
476 temperature on the airflow pattern and air velocity profile was observed. The presence and
477 absence of a space underneath the product led to similar temperatures, despite the difference
478 in airflow pattern in the case of PCM on the side.

479 It is recommended that the PCM should be placed at the top of the box in order to reduce
480 temperature stratification. This configuration has been previously investigated in an empty
481 cavity and this work confirms, by experiment, that it can be applied for the loaded cavity as
482 well. The box should not be too high to avoid a high temperature and large temperature
483 heterogeneity. The effect of aspect ratio is complex as higher boxes allow higher convective
484 heat transfer and also higher thermal stratification. Thus, CFD model is suggested to analyze in
485 detail the influence of aspect ratio on temperature distribution. To maintain the product
486 temperature along a supply chain, PCM could be placed on all walls (top, bottom, sidewalls);
487 however, the available volume would be significantly reduced and the logistic cost per kg of
488 product would be higher. Our study demonstrates that it is possible to place PCM only at one

489 wall (top or side) if an appropriate PCM mass is used. This mass depends on the ambient
490 temperature in the supply chain, which directly impacts airflow and product temperature.
491 Hence, the ambient temperature is an important factor for the system design, i.e., box wall
492 material, PCM type and mass. However, linear extrapolation from one ambient to another is
493 not recommended because of non-linear behavior, thus physical based models taking natural
494 convection into account should be used to analyze the impact of ambient temperature on product
495 temperature in an insulated box with PCM. Loading a product at a high temperature should be
496 avoided since it takes more than 10 hours to cool it down according to its high thermal inertia.
497 Adding a 20-mm air space beneath the test product neither reduces the test product temperature
498 nor increases homogeneity although this gap allows slightly better air circulation. Future studies
499 are required to determine the influence of the other air gaps: between PCM and load, between
500 lateral and top walls and load. The use of PCM can delay the internal temperature evolution
501 and the amount of PCM linearly correlates with the maximum storage time of the insulated box.
502 The influence of other parameters like the amount of product and the emissivity of box walls
503 will be studied.

504 The experimental velocity and temperature fields obtained in different conditions can further
505 be used to validate CFD models. They should confirm that when PCM is at top, although the
506 configuration is symmetric, the velocity and temperature fields can be asymmetric. In practice,
507 there are many other possible box designs and operating conditions and the interactions between
508 the different factors are complex. Thus, numerical models are necessary for investigating the
509 influence of these factors on temperature distribution and evolution in a wide variety of
510 configurations (e.g., smaller/larger boxes, improved insulation). The experimental results
511 presented in the present article can contribute to validate these models.

512 **Acknowledgement**

513 King Mongkut's Institute of Technology Ladkrabang, Thailand (contract no. KREF156402),
514 French Embassy in Thailand, and the National Research Institute for Agriculture, Food and
515 Environment, France are gratefully acknowledged for their financial support. The authors
516 would also like to thank the Royal Thai Government Scholarship and Chulalongkorn
517 University, Bangkok, Thailand for T. Leungtongkum's PhD scholarship. This research did not
518 receive any specific grant from funding agencies in the public, commercial, or not-for-profit
519 sectors. Thanks to LaVision for PIV technical support.

520 **References**

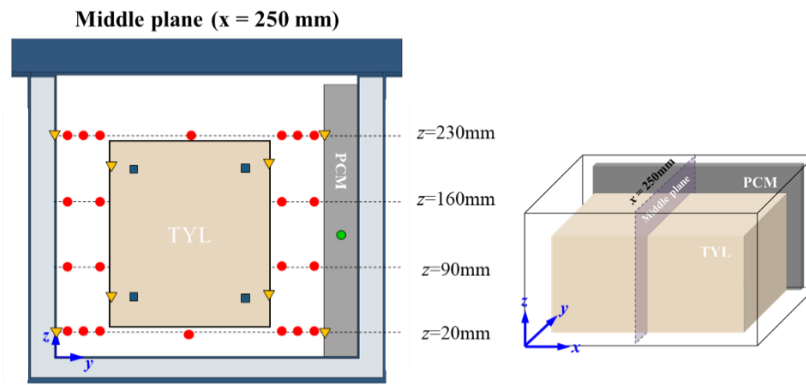
- 521 Ataei-Dadavi, I., Chakkingal, M., Kenjeres, S., Kleijn, C. R., & Tummers, M. J. (2019). Flow
522 and heat transfer measurements in natural convection in coarse-grained porous media.
523 *International Journal of Heat and Mass Transfer*, 130, 575–584.
524 <https://doi.org/10.1016/j.ijheatmasstransfer.2018.10.118>
- 525 Bergman, T. L., Lavine, A. S., Incropera, F. P., & DeWitt, D. P. (2011). *Introduction to Heat*
526 *Transfer*. John Wiley & Sons.
- 527 Burgess, S., Wang, X., Rahbari, A., & Hangi, M. (2022). Optimisation of a portable phase-
528 change material (PCM) storage system for emerging cold-chain delivery applications.
529 *Journal of Energy Storage*, 52, 104855. <https://doi.org/10.1016/j.est.2022.104855>
- 530 Calati, M., Righetti, G., Zilio, C., Hooman, K., & Mancin, S. (2023). CFD analyses for the
531 development of an innovative latent thermal energy storage for food transportation.
532 *International Journal of Thermofluids*, 17, 100301.
533 <https://doi.org/10.1016/j.ijft.2023.100301>
- 534 Cengel, Y. A., & Ghajar, A. J. (2020). *Heat and Mass Transfer: Fundamentals &*
535 *Applications*. McGraw-Hill Education.
- 536 Choi, C., Cho, H. W., Ha, M. Y., & Yoon, H. S. (2015). Effect of circular cylinder location on
537 three-dimensional natural convection in a cubical enclosure. *Journal of Mechanical*

- 538 *Science and Technology*, 29(3), 1307–1318. [https://doi.org/10.1007/s12206-015-0246-](https://doi.org/10.1007/s12206-015-0246-3)
539 3
- 540 Du, J., Nie, B., Zhang, Y., Du, Z., Wang, L., & Ding, Y. (2020). Cooling performance of a
541 thermal energy storage-based portable box for cold chain applications. *Journal of*
542 *Energy Storage*, 28, 101238. <https://doi.org/10.1016/j.est.2020.101238>
- 543 Icier, F., & Ilicali, C. (2005). The use of tylose as a food analog in ohmic heating studies.
544 *Journal of Food Engineering*, 69(1), 67–77.
545 <https://doi.org/10.1016/j.jfoodeng.2004.07.011>
- 546 Kacimi, A., & Labranque, G. (2019). Combination of vacuum insulation panels and phase
547 change materials in temperature-controlled containers. *Proceedings of the 25th IIR*
548 *International Congress of Refrigeration: Montréal, Canada, August 24-30, 2019*.
549 <https://doi.org/10.18462/iir.icr.2019.0163>
- 550 Labihi, A., Aitlahbib, F., Chehouani, H., Benhamou, B., Ouikhalfan, M., Croitoru, C., &
551 Nastase, I. (2017). Effect of phase change material wall on natural convection heat
552 transfer inside an air filled enclosure. *Applied Thermal Engineering*, 126, 305–314.
553 <https://doi.org/10.1016/j.applthermaleng.2017.07.112>
- 554 Laguerre, O., Derens, E., & Flick, D. (2018). Modelling of fish refrigeration using flake ice.
555 *International Journal of Refrigeration*, 85, 97–108.
556 <https://doi.org/10.1016/j.ijrefrig.2017.09.014>
- 557 Laguerre, O., & Flick, D. (2004). Heat transfer by natural convection in domestic
558 refrigerators. *Journal of Food Engineering*, 62(1), 79–88.
559 [https://doi.org/10.1016/S0260-8774\(03\)00173-0](https://doi.org/10.1016/S0260-8774(03)00173-0)
- 560 Lee, S. H., Seo, Y. M., Yoon, H. S., & Ha, M. Y. (2016). Three-dimensional natural
561 convection around an inner circular cylinder located in a cubic enclosure with

- 562 sinusoidal thermal boundary condition. *International Journal of Heat and Mass*
563 *Transfer*, 101, 807–823. <https://doi.org/10.1016/j.ijheatmasstransfer.2016.05.079>
- 564 Leporini, M., Corvaro, F., Marchetti, B., Polonara, F., & Benucci, M. (2018). Experimental
565 and numerical investigation of natural convection in tilted square cavity filled with air.
566 *Experimental Thermal and Fluid Science*, 99, 572–583.
567 <https://doi.org/10.1016/j.expthermflusci.2018.08.023>
- 568 Leungtonkum, T., Flick, D., Hoang, H. M., Steven, D., Delahaye, A., & Laguerre, O. (2022).
569 Insulated box and refrigerated equipment with PCM for food preservation: State of the
570 art. *Journal of Food Engineering*, 317, 110874.
571 <https://doi.org/10.1016/j.jfoodeng.2021.110874>
- 572 Leungtonkum, T., Laguerre, O., Flick, D., Denis, A., Duret, S., & Chaomuang, N. (2023a).
573 Experimental investigation of airflow and heat transfer by natural convection in an
574 insulated box with a Phase Change Material using a Particle Image Velocimetry
575 technique. *Journal of Food Engineering*, 336, 111207.
576 <https://doi.org/10.1016/j.jfoodeng.2022.111207>
- 577 Leungtonkum, T., Laguerre, O., & Flick, D. (2023b). Simplified heat transfer model for real-
578 time temperature prediction in insulated boxes equipped with a phase change material.
579 *International Journal of Refrigeration*, 149, 286–298.
580 <https://doi.org/10.1016/j.ijrefrig.2023.02.009>
- 581 Margeirsson, B., Pálsson, H., Popov, V., Gospavic, R., Arason, S., Sveinsdóttir, K., &
582 Jónsson, M. Þór. (2012). Numerical modelling of temperature fluctuations in
583 superchilled fish loins packaged in expanded polystyrene and stored at dynamic
584 temperature conditions. *International Journal of Refrigeration*, 35(5), 1318–1326.
585 <https://doi.org/10.1016/j.ijrefrig.2012.03.016>

- 586 Miroshnichenko, I. V., & Sheremet, M. A. (2018). Turbulent natural convection heat transfer
587 in rectangular enclosures using experimental and numerical approaches: A review.
588 *Renewable and Sustainable Energy Reviews*, 82, 40–59.
589 <https://doi.org/10.1016/j.rser.2017.09.005>
- 590 Moreno, S., Hinojosa, J. F., Hernández-López, I., & Xaman, J. (2020). Numerical and
591 experimental study of heat transfer in a cubic cavity with a PCM in a vertical heated
592 wall. *Applied Thermal Engineering*, 178, 115647.
593 <https://doi.org/10.1016/j.applthermaleng.2020.115647>
- 594 Ohkawara, H., Kitagawa, T., Fukushima, N., Ito, T., Sawa, Y., & Yoshimine, T. (2012). A
595 Newly Developed Container for Safe, Easy, and Cost-effective Overnight
596 Transportation of Tissues and Organs by Electrically Keeping Tissue or Organ
597 Temperature at 3 to 6°C. *Transplantation Proceedings*, 44(4), 855–858.
598 <https://doi.org/10.1016/j.transproceed.2012.02.023>
- 599 Paquette, J.-C., Mercier, S., Marcos, B., & Morasse, S. (2017). Modeling the thermal
600 performance of a multilayer box for the transportation of perishable food. *Food and*
601 *Bioproducts Processing*, 105, 77–85. <https://doi.org/10.1016/j.fbp.2017.06.002>
- 602 Raffel, M., Willert, C., Wereley, S., & Kompenhans, J. (2007). *Particle Image Velocimetry: A*
603 *Practical Guide*. <https://doi.org/10.1007/978-3-540-72308-0>
- 604 Rahimi-Khoigani, S., Hamdami, N., & Dalvi-Isfahan, M. (2023). Application of an improved
605 latent heat storage system in the food packaging. *Journal of Food Engineering*, 341,
606 111351. <https://doi.org/10.1016/j.jfoodeng.2022.111351>
- 607 Raithby, G. D., & Hollands, K. G. T. (1998). Natural convection. In W. M. Rohsenow, J. P.
608 Hartnett, & Y. I. Cho, *Handbook of Heat Transfer* (3rd ed). McGraw-Hill.
- 609 Rincón-Casado, A., Sánchez de la Flor, F. J., Chacón Vera, E., & Sánchez Ramos, J. (2017).
610 New natural convection heat transfer correlations in enclosures for building

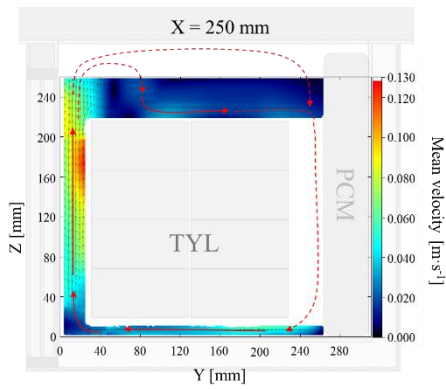
- 611 performance simulation. *Engineering Applications of Computational Fluid Mechanics*,
612 *11*(1), 340–356. <https://doi.org/10.1080/19942060.2017.1300107>
- 613 Xiaofeng, X., & Xuelai, Z. (2021). Simulation and experimental investigation of a multi-
614 temperature insulation box with phase change materials for cold storage. *Journal of*
615 *Food Engineering*, *292*, 110286. <https://doi.org/10.1016/j.jfoodeng.2020.110286>
- 616 Zhang, X., Su, G., Yu, J., Yao, Z., & He, F. (2015). PIV measurement and simulation of
617 turbulent thermal free convection over a small heat source in a large enclosed cavity.
618 *Building and Environment*, *90*, 105–113.
619 <https://doi.org/10.1016/j.buildenv.2015.03.015>
- 620 Zhao, X., Xia, M., Wei, X., Xu, C., Luo, Z., & Mao, L. (2019). Consolidated cold and
621 modified atmosphere package system for fresh strawberry supply chains. *LWT*, *109*,
622 207–215. <https://doi.org/10.1016/j.lwt.2019.04.032>
- 623



624

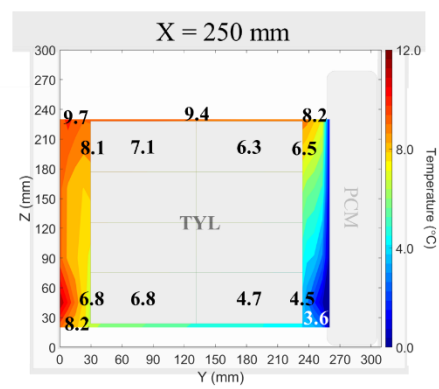
625 **Figure 1:** Experimental setup and thermocouple positions in the horizontal box with PCM on
626 a side wall and loaded with the test product (Tylose, TYL). Note: Similar setup and measured
627 positions were applied for the vertical box.

Air velocity field

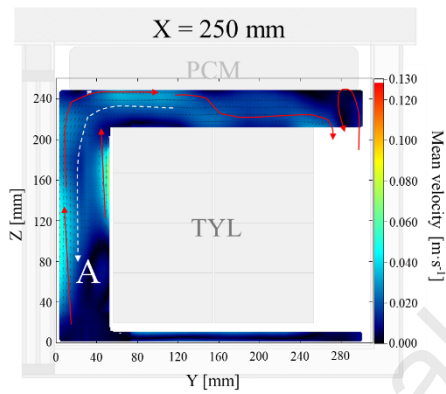


(a)

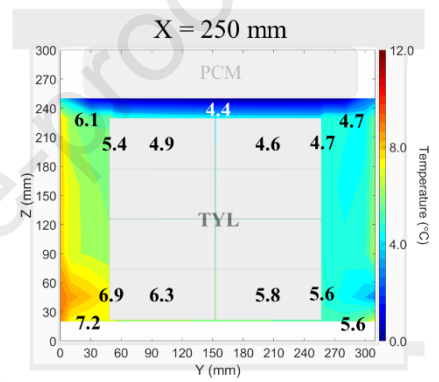
Temperature field



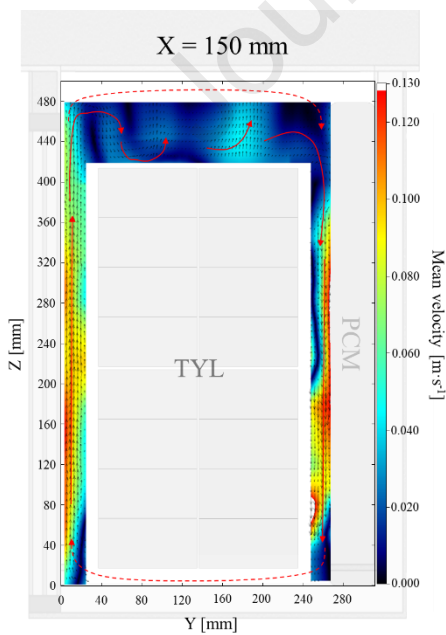
(a')



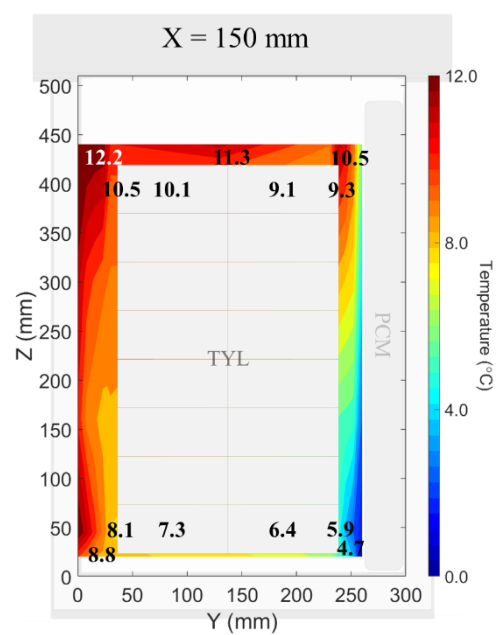
(b)



(b')



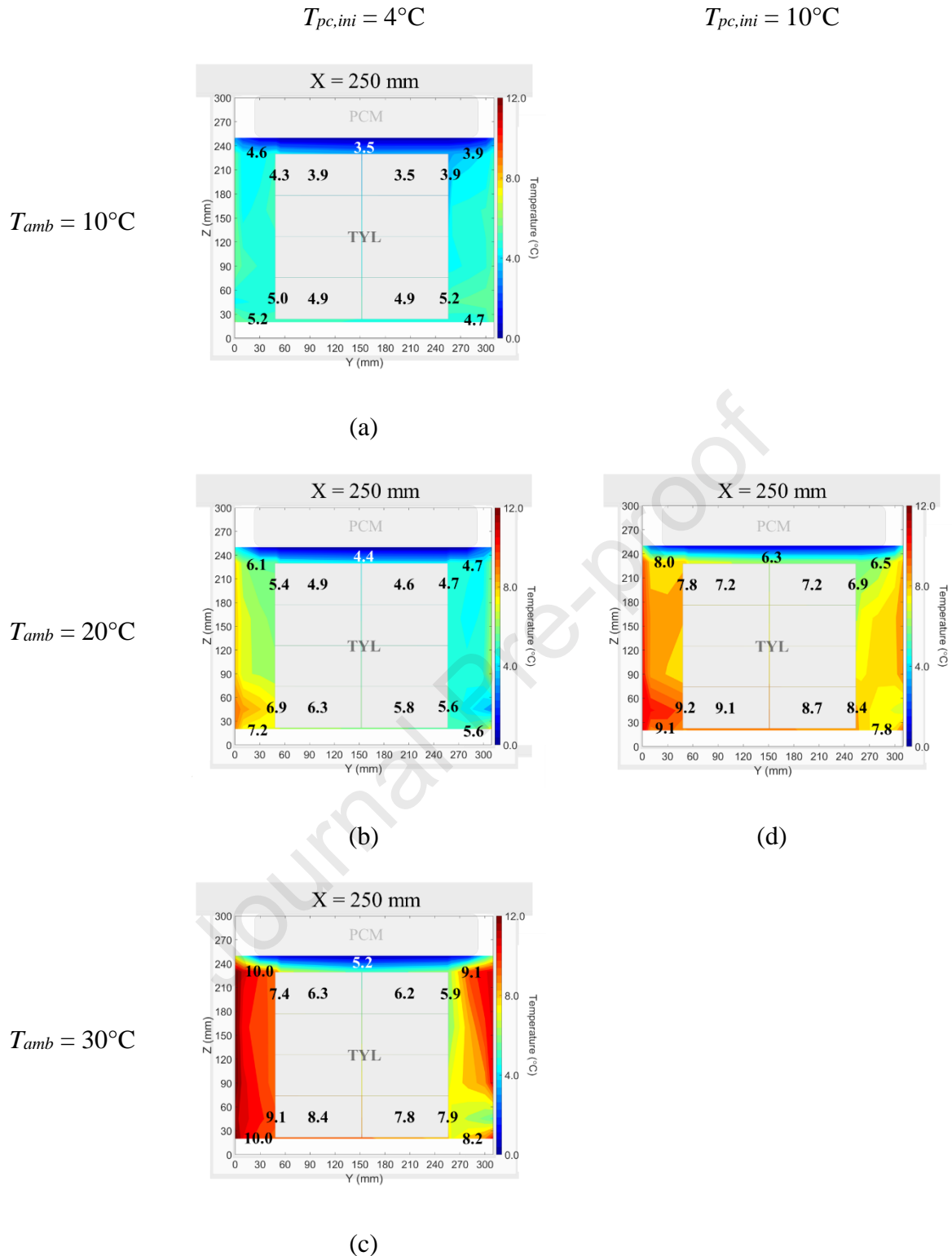
(c)



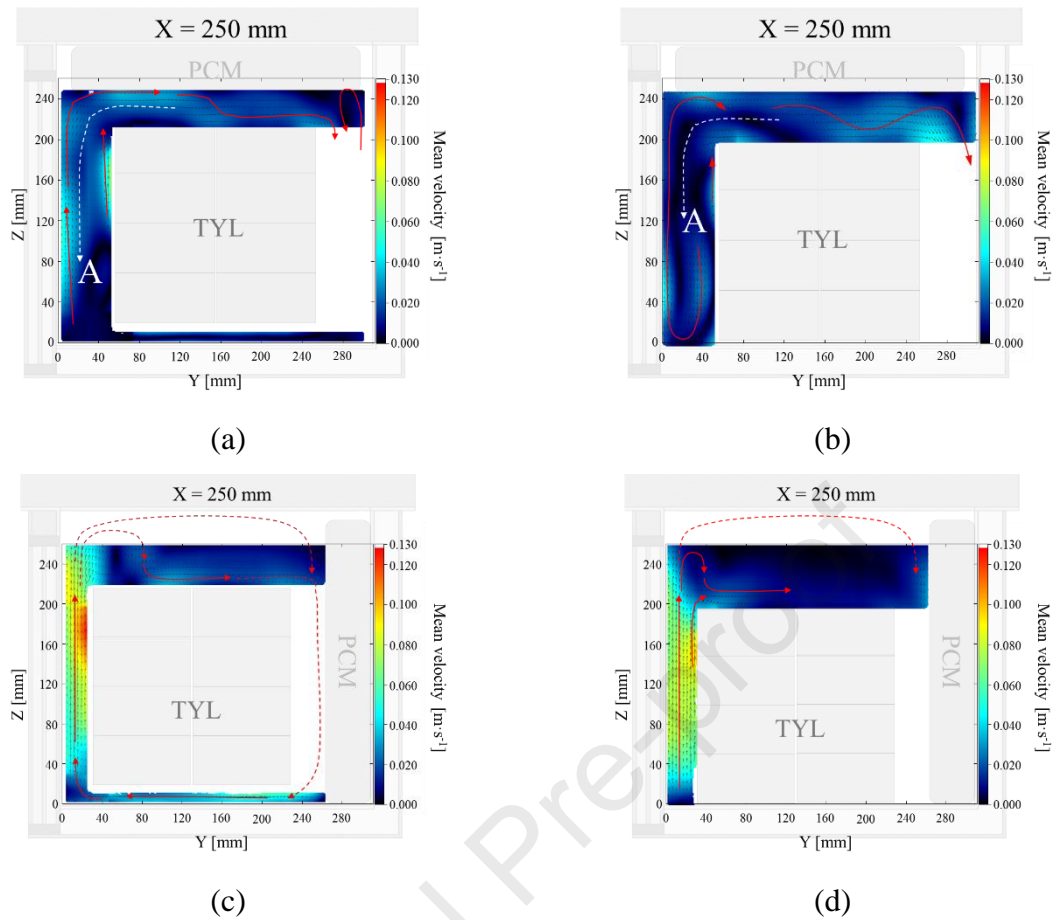
(c')

628 **Figure 2:** Measured air velocity field on the middle plane of a loaded box with (a) PCM on
629 the side of the horizontal box; (b) PCM at the top of the horizontal box; and (c) PCM on the
630 side of the vertical box. (a'), (b') and (c') are corresponding measured temperature fields (for
631 one of the replications)

Journal Pre-proof

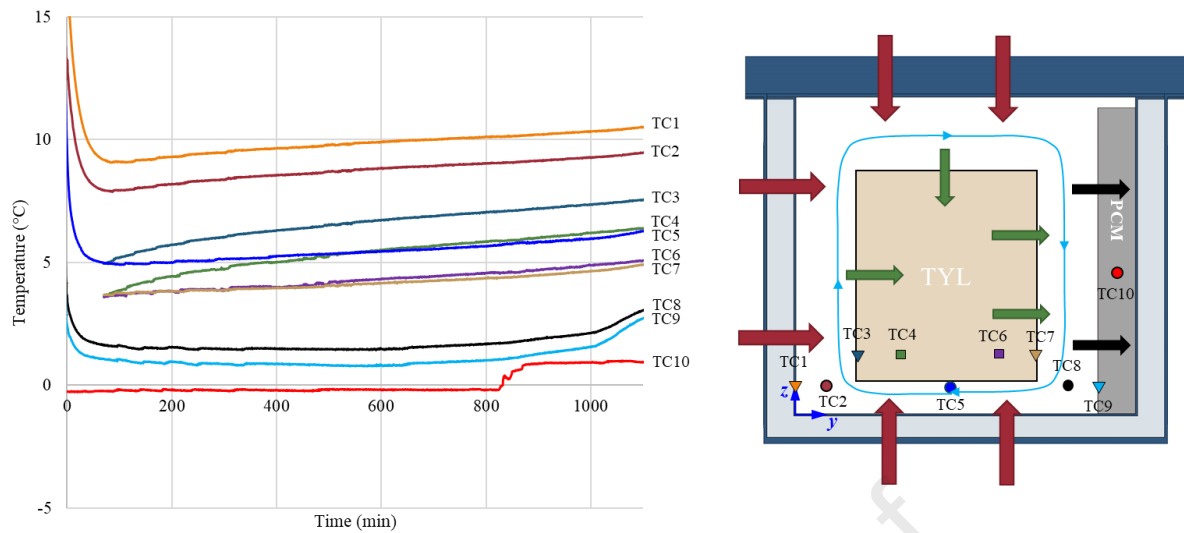


632 **Figure 3:** Measured temperature field on the middle plane of a loaded box with PCM at the
 633 top and a product initial temperature of 4°C under (a) 10°C ambient temperature; (b) 20°C
 634 ambient temperature; (c) 30°C ambient temperature; and (d) product initial temperature of
 635 10°C under 20°C ambient temperature



636 **Figure 4:** Measured air velocity field on the middle plane of a loaded box (a) PCM at the top,
 637 20-mm gap underneath the test product, (b) PCM at the top, without gap, (c) PCM on the
 638 side, 20-mm gap underneath the test product and (d) PCM on the side, without gap

639



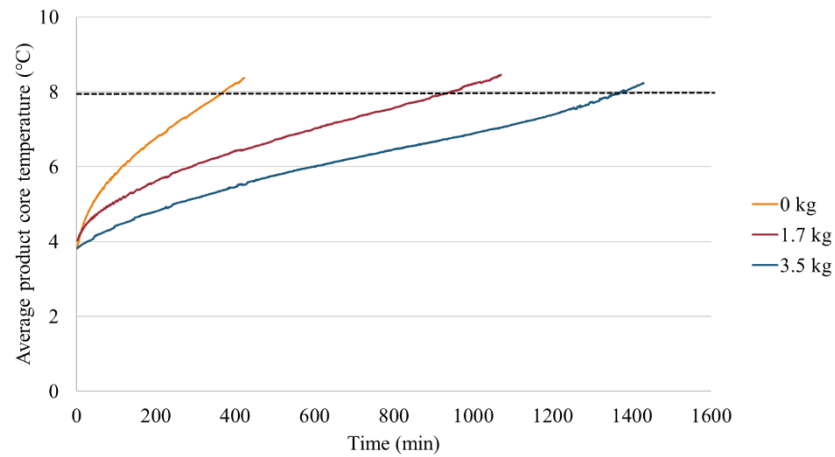
640

641 **Figure 5:** Temperature evolution at the bottom of the box during experiment No. 1 (ambient

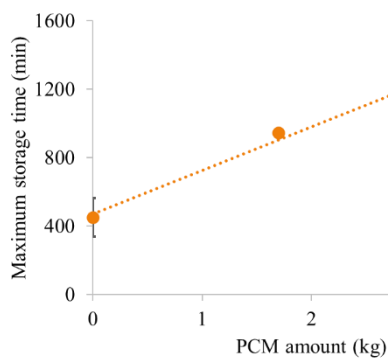
642 temperature = 20°C and initial test product temperature = 4°C) with heat flow (red arrows –

643 from ambient, green arrows – between the internal air and the test product, and black arrows –

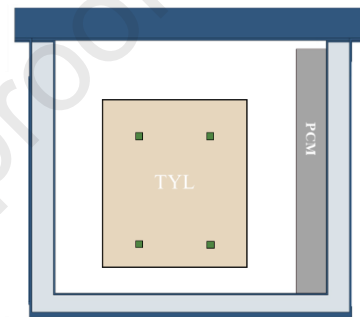
644 from the internal air to the PCM). Airflow shown using blue arrows



(a)



(b)



645

646 **Figure 6:** Effect of the amount of PCM on (a) test product core temperature evolution; and

647 (b) maximum storage time, t_{max} . Error bars represent the standard deviation of 2 replications.

648 The experiment was conducted under condition 4: loaded box with PCM on a sidewall with

649 an ambient temperature of 20°C, 4°C initial product temperature, 20 mm gap beneath the test

650

product (Tylose, TYL)

651

652

Table 1: Thermophysical properties of materials

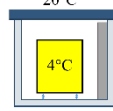
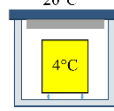
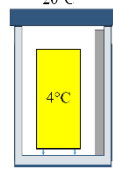
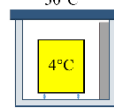
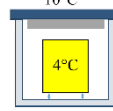
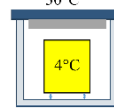
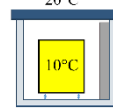
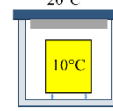
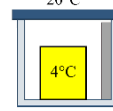
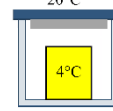
Material	ρ (kg·m⁻³)	C_p (J·kg⁻¹·K⁻¹)	λ (W·m⁻¹·K⁻¹)	Reference
Liquid water	1000	4217	0.561	Cengel & Ghajar (2020)
*Ice	920	2040	1.880	Cengel & Ghajar (2020)
Test product (Tylose)	1070	3372	0.510	Icier & Ilicali (2005)

653 *Enthalpy of melting of ice (L_f) is 333700 J/kg with melting temperature (T_m) at 0°C

Journal Pre-proof

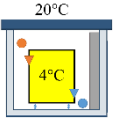
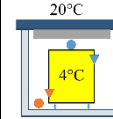
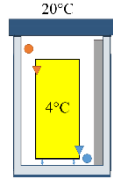
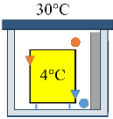
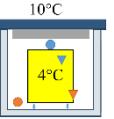
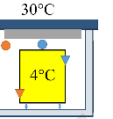
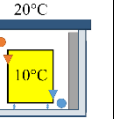
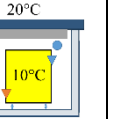
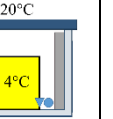
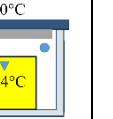
654

Table 2: Experimental conditions

Condition	1*	2*	3	4	5	6	7	8	9*	10*
										
PCM position	Side	Top	Side	Side	Top	Top	Side	Top	Side	Top
Aspect ratio	~1	~1	1.7	~1	~1	~1	~1	~1	~1	~1
Ambient temperature (°C)	20	20	20	30	10	30	20	20	20	20
Initial test product temperature (°C)	4	4	4	4	4	4	10	10	4	4
Spacing beneath test product (mm)	20	20	20	20	20	20	20	20	0	0

655 * with two replications

656 **Table 3:** Test product core, surface and internal air temperatures for all experimental loaded conditions. Note: the reported values are the
 657 average of the temperatures measured between 400 min. and 600 min. considered as the stable thermal condition.

	Condition	***1	***2	3	4	5	6	7	8	***9	***10	**SD
	*Pictogram	20°C 	20°C 	20°C 	30°C 	10°C 	30°C 	20°C 	20°C 	20°C 	20°C 	
Core temperature	Average	5.8 (5.6,6.0)	5.4 (5.3,5.4)	7.8	7.4	4.3	7.2	9.3	8.0	5.8 (5.7,5.8)	5.6 (5.4,5.7)	0.19
	Minimum	4.5 (4.2,4.8)	4.6 (4.5,4.6)	6.2	5.4	3.5	6.2	7.4	7.2	4.5 (4.4,4.6)	4.2 (4.1,4.3)	-
	Maximum	6.8 (6.6,7.1)	6.4 (6.3,6.4)	9.5	9.4	4.9	8.4	10.9	9.1	6.5 (6.4,6.6)	7.0 (6.8,7.1)	-
Surface temperature	Average	6.3 (6.1,6.5)	5.5 (5.3,5.7)	8.1	8.5	4.6	7.6	9.0	8.1	6.0 (6.1,5.9)	5.7 (5.6,5.8)	0.22
	Minimum	4.3 (4.1,4.5)	4.6 (4.4,4.7)	5.8	5.2	3.9	5.9	6.0	6.9	3.7 (3.4,3.9)	4.4 (4.2,4.5)	-
	Maximum	7.7 (7.3,8.1)	6.6 (6.4,6.9)	9.9	10.7	5.2	9.1	11.0	9.2	7.5 (7.2,7.8)	7.2 (7.0,7.3)	-
Internal air temperature	Average	6.6 (6.2,7.0)	5.7 (5.7,5.7)	8.5	10.0	4.7	9.1	8.7	8.0	6.4 (6.0,6.7)	5.6 (5.5,5.7)	0.38
	Minimum	2.6 (1.5,3.6)	4.5 (4.4,4.6)	4.7	4.6	3.5	5.2	4.1	6.3	1.6 (1.2,2.0)	4.4 (4.4,4.4)	-
	Maximum	8.6 (7.7,9.6)	7.0 (6.9,7.2)	12.2	13.3	5.2	10.0	10.7	9.1	8.9 (8.9,8.9)	7.0 (6.9,7.0)	-
	**SD	2.2	1.1	3.0	3.0	0.5	1.6	2.3	0.9	2.5	1.0	-

658 *▼ and ▼ represent the coldest and warmest locations in the test product, respectively while ● and ● signify the coldest and warmest locations
 659 in the air, respectively.

- 660 ** SD = Standard Deviation (°C). For a given condition (each column), SD represents the variation of air temperature among 13 measurement
661 positions. For a given temperature (same row), SD represents the variation of temperature measured at 4 positions between 2 replications.
- 662 *** The values in parenthesis were the results of each replication.

Journal Pre-proof

Declaration of interests

The authors declare that they have no known competing financial interests or personal relationships that could have appeared to influence the work reported in this paper.

The authors declare the following financial interests/personal relationships which may be considered as potential competing interests:

Journal Pre-proof